AIAA 80-1000R

Analysis of Interior Noise-Control Treatments for High-Speed Propeller-Driven Aircraft

J. D. Revell* and F. J. Balena†
Lockheed-California Company, Burbank, Calif.
and
L. R. Koval‡
University of Missouri, Rolla, Mo.

An analytical method is described for prediction of the interior noise levels for propeller-driven aircraft, given the exterior noise signature, its harmonic spectrum, and a description of the fuselage sidewall structure and various candidate "add-on" noise-control elements. The structural response is described by the theory of Koval, but simplified to consider the stiffeners as "smeared" elements. The incremental transmission loss (TL) due to add-on noise-control elements is derived from the Beranek and Work method. Comparisons between experimental data and the theory are presented. The method is reasonably accurate below the ring frequency, but is somewhat conservative at the normal incidence angle. This method is, however, expedient computationally, is economical, and permits rapid comparisons of noise-control penalties for various treatment concepts.

Introduction

THIS paper describes the method of analysis, and a companion paper[1] describes a sample of the results, of a lengthy study for NASA Langley of interior noise control for propfan-powered aircraft.[2] Reference 1 shows the necessary mass penalties for achieving an interior noise level of 80 dBA for three different sized aircraft. These studies are in support of the NASA effort to develop technology readiness for propfan-powered aircraft of the future, which promise fuel savings of nearly 20% relative to turbofan-powered aircraft having otherwise comparable technology.[3] The studies in Refs. 1 and 2 show that mass penalties for cabin noise control range from 1 to 2.5% of the takeoff gross weight (TOGW) of the various aircraft. According to Ref. 3, the percentage of block fuel saving is degraded by about the same amount; therefore an efficient fuselage sidewall design is required to minimize the mass penalties for cabin noise control. The method described in this paper is considered to be a useful tool for the analysis of such noise-control designs.

Qualitative Description of the Interior Noise Prediction Procedure

Determination of Overall Sound Pressure Levels and A-Weighted Interior Sound Pressure Levels

Required Input Data

The method assumes knowledge of the external distribution of the free-field overall sound pressure level (OASPL) caused by each propeller, and the relative sound pressure levels (SPL) for the first ten harmonics of the blade passage frequency for a given aircraft configuration.

The fuselage sidewall structural properties (stiffness of rings and stringers, etc.); the available space between the inner wall (trim panel) and outer skin; the necessary minimum fiberglass blanket thickness; and the variation of interior absorption coefficient with frequency must be known. Figure 1 shows a typical sidewall configuration. The relative tip clearance of the propeller must be known to determine the angle of incidence associated with the external sound pressure amplitudes defined by the external signature from each engine. The companion paper[1] shows three different external propeller harmonic spectra which were studied.

Procedure for Calculating Interior Levels

The spectrum of sidewall noise reduction (NR) is calculated from the following relationship:

$$NR = 10 \log (1 + \alpha/\tau) \quad (1)$$

where τ is the transmission coefficient at frequency f, and α (f) is the absorption coefficient at f. The absorption coefficient schedule is given in Ref. 2, typically $\alpha = 0.13$ at 164 Hz and 0.22 at 328 Hz. The frequencies are representative of the blade passage frequency (BPF) and twice the BPF for a typical propfan application.

The transmission coefficient τ and the transmission loss (TL) are related by

$$TL = -10 \log \tau \quad (2)$$

When the NR is known, then the interior SPL value at each of the harmonics is computed by subtracting the NR at the corresponding blade passage frequency harmonic from the

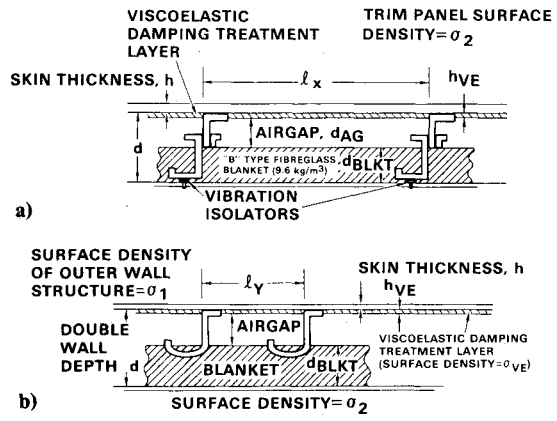

Fig. 1 Generalized sidewall construction. a) Cross section of frames. b) Cross section of stringers.

Presented as Paper 80-1000 at the AIAA 6th Aeroacoustics Conference, Hartford, Conn., June 4-6, 1980; submitted July 23, 1980; revision received April 21, 1981.

*R&D Scientist, Acoustics Department. Associate Fellow AIAA.
†R&D Engineer, Acoustics Department.
‡Professor, Department of Mechanical and Aerospace Engineering. Member AIAA.

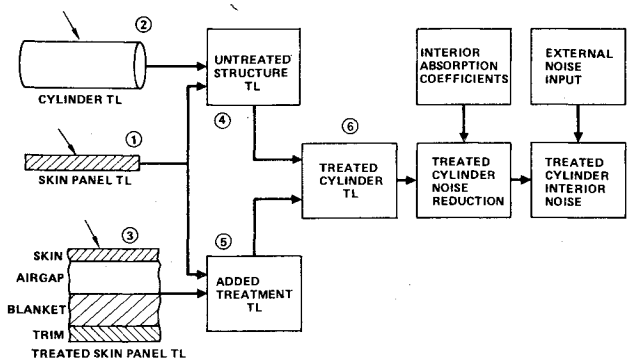

Fig. 2 Method used to calculate treated cylinder.

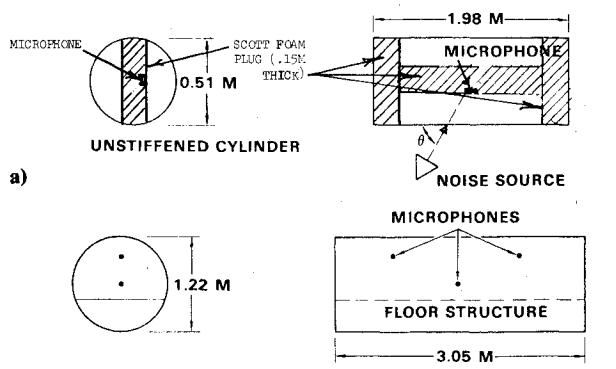

Fig. 3 Cylinder noise reduction test layouts. a) Free field-anechoic chamber. b) Random incidence-reverberant field.

Table 1 Structural properties of test cylinders

	Anechoic chamber test specimen	Reverberation room test specimen
Cylinder diameter, m (in.)	0.51 (20)	1.22 (48)
Skin gage, cm (in.)	0.081 (0.032)	0.127 (0.050)
Cylinder length, m (in.)	0.183 (72)	3.05 (120)
Frame spacing, m (in.)	NA	0.46 (18)
Frame area, cm^2 ($in.^2$)	NA	0.50 (0.0768)
Frame centroidal distance, re: skin, cm (in.)	NA	1.32 (0.521)
Frame second moment of inertia, re: skin, cm^4 ($in.^4$)	NA	1.54 (0.037)

exterior SPL. When the interior SPL is known at each frequency, the interior OASPL, A-weighted SPL (dBA), and speech interference level (SIL) can be calculated in a straightforward manner insofar as the contributions of the propeller alone are concerned. It should be noted that the dBA and SIL levels will be impacted by other sources, such as the cabin environmental control system (ECS) and by the transmission of boundary-layer noise in regions away from the propeller noise treatment area. Therefore any excessively low predictions for dBA and SIL should be checked for limits imposed by these other effects.

Determination of Transmission Loss

General Outline

Figure 2 shows schematically the method used, which is further explained in the following steps. First calculate the TL of the untreated structure, then compute the incremental TL due to the sidewall elements. The untreated structure TL is taken to be the lower envelope of either the cylindrical shell TL as computed by Koval's theory with the stiffeners smeared to achieve an equivalent monocoque shell,[4,5] or the TL of the small flat skin panel which is bounded by the stiffeners according to Cockburn and Jolly.[6] Appendices A, B, and C summarize the pertinent equations.

The use of the "lower bound" of either the shell or the panel TL is intended as a simplified and conservative engineering procedure, in lieu of more complex computations coupling the panels and shell together. The main justification is the cost effectiveness and empirical justification for the accuracy, as will be discussed later.

The incremental TL due to the sidewall treatments is calculated via the method of Beranek and Work[7] as implemented by Cockburn and Jolly (after several corrections detailed in Ref. 2). This incremental TL due to the treatment is then added to the untreated structure TL shown in Fig. 2. Appendix B describes the key equations for defining the TL of multilayer flat walls. The incremental TL used in this study is defined as the difference between the TL of the multilayer flat wall and the TL of the bare (flat) skin panel. This procedure is considered valid when the acoustic wavelengths are large compared to the panel dimensions, which is the situation encountered for low-frequency propeller noise.

Comparison of the Method with Experimental Data Noise Reduction

Small Cylinder Tests

Figure 3 shows the setup for two kinds of noise-reduction tests on small cylinders conducted at the Lockheed Rye Canyon Acoustics Laboratory. Figure 3a shows free-field anechoic chamber tests on a 0.51-m (20-in.) unstiffened cylinder subjected to oblique plane-wave acoustical excitation. Figure 3b shows the setup for a 1.22-m (4-ft) diam ring-stiffened cylinder in a large reverberation chamber.

Table 1 shows the structural properties of the test cylinders in Figs. 3a and 3b.

Figures 4a-c show results of the simulated oblique plane-wave tests on the 0.51-m (20-in.) cylinder at graze angles of 45, 60, and 90 deg. Both ends of the cylinder were treated with a 0.15-m (6-in.) thickness of Scott Foam and lead vinyl. Also, a 0.15-m (6-in.) thick center plug of Scott Foam ran the entire length of the cylinder, as shown in Fig. 3a. The average absorption coefficient of the foam was 64% for frequencies above 300 Hz. The purpose of using the high absorption center plug was to minimize the difference between noise reduction and transmission loss in accordance with Eq. (1), thus providing, as closely as possible, a test of the transmission loss theory of Koval (Refs. 4 and 5). Noise reduction was determined by the insertion loss method, measuring the difference between the sound pressure inside the cylinder and the free-field sound pressure at the same location when the cylinder is absent.

Figure 5 shows results for the stiffened 1.22-m (4-ft) cylinder in the reverberation room, with and without a floor. The calculations show two different assumed values of absorption coefficient.

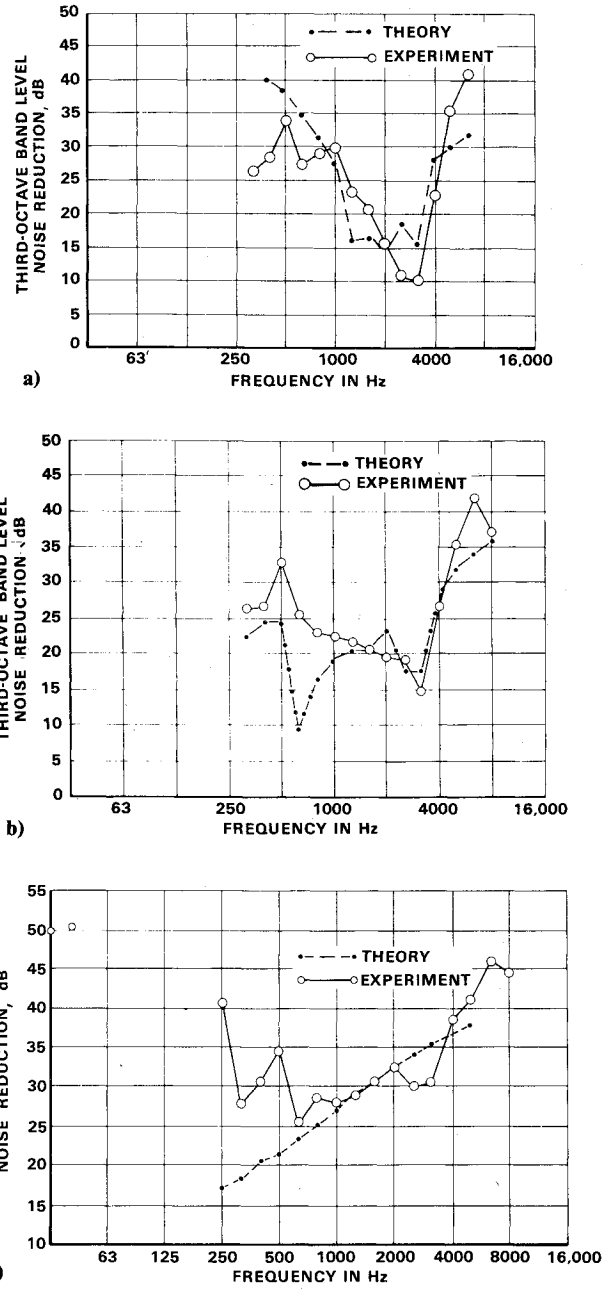

Fig. 4 Noise reduction test on 20-in. cylinder in anechoic chamber: a) 45-deg grazing angle. b) 60-deg grazing angle. c) 90-deg grazing angle.

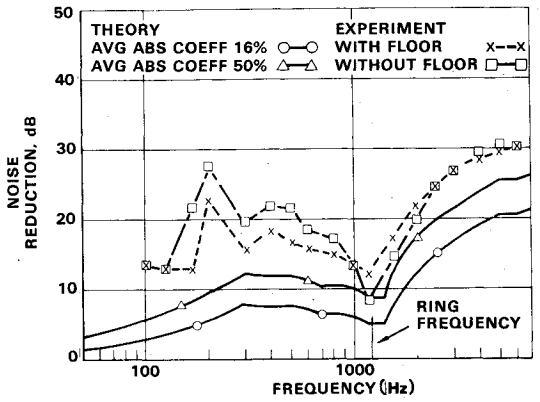

Fig. 5 Theoretical vs experimental noise reduction: 4-ft-diam stiffened cylinder in reverberation chamber.

Multilayer Panel Transmission Loss Test

Figures 6a and 6b show TL results for two layered sidewall configurations which have a 2.4-kg/m^2 (0.50-psf) lead vinyl septum terminating the wall, thus simulating a trim panel. These test panels were installed in the wall between a large and small reverberation room. The test panel was flat; the lateral dimensions 2.4×2.4 m (8×8 ft), with typical aircraft frames spaced at 0.51 m (20 in.) and no stringers. The outer aluminum skin facing the source was aluminum 0.18 cm (0.070 in.) thick. A broadband, random noise source was used in the larger reverberation room, 7.9×16.1×6.1 m (26×53×20 ft), located in the corner opposite to the test panel.

Discussion

Cylindrical Shell Noise Reduction Results

The results for unstiffened cylindrical shells with oblique plane-wave excitation shown in Figs. 6a-c show the following trends. At the lowest grazing angle (45 deg), the theoretical low-frequency NR values are higher than experimental values. The ring frequency, f_R, is defined as the longitudinal wave speed in the shell divided by circumference. Its value is 3247 Hz for the 20-in. diam cylinder. For 45 deg, the theory overpredicts NR at frequencies below one-third of the ring frequency. At frequencies above 33% and below 200% of the ring frequency, the experimental NR agrees with the theory. Above twice the ring frequency, the theory underpredicts the NR.

At the important case of normal incidence (90-deg grazing angle) the theory agrees well with test data above 20% of the ring frequency; however, between 8% f_R (250 Hz) and 20% f_R, the theory underpredicts NR by an increasing margin, varying from 10 to 20 dB at the lowest frequencies. Some possible explanations for the principal experimental discrepancies are given in the last three paragraphs under Concluding Remarks.

Test results shown in Fig. 5 for the 1.22-m (4-ft) stiffened cylinder in the reverberant chamber are now considered. The theoretical results for the 16% absorption coefficient show a systematic underprediction of at least 5 dB, which can be eliminated by assuming a higher absorption coefficient value of 50%, bringing the results in agreement at the ring frequency. However, the interior absorption material is applied only to the ends of the test cylinder, comprising only 15% of the surface area of the cylinder. The estimated true surface absorption coefficient is 64%; therefore the net absorption coefficient when referred to the transmitting area is only about 10%. The calculated transmission coefficient averaged over a classical incidence angle range of from −87.5 to +87.5 deg is given by Cremer's result,[8]

$$\tau = 2\int_0^{\theta'} (\theta)\sin(2\theta)\,\mathrm{d}\theta/(1-\cos 2\theta') \qquad (3)$$

where $\theta' = 87.5$ deg in this case. The reader will note that the classical incidence angle θ' in Eq. (3) is equal to 90 deg minus the grazing angle referred to in Fig. 7 and in Eqs. (A3-A18) of Appendix A, which summarize Koval's theory preserving the notation of Refs. 4 and 5. From Eq. (3), it is seen that the random incidence transmission coefficient tends to be dominated by transmission between incidence angles of zero, where transmission is high, and at 45 deg, where the weighting is high; therefore the results in Fig. 5 are like an average of those in Figs. 4a-c for plane waves at grazing angles between 45 and 90 deg. The pattern is the same: at and above the ring frequency [1353 Hz for the 1.22-m (4-ft) cylinder] the frequency variation trend shows good agreement between theory and experiment. Below the ring frequency, the theory underpredicts the test data (without the floor) by as much as 10 dB at frequencies below one-half the ring frequency. It is noted that the presence of the floor decreases the low-frequency noise reduction, which may be consistent with some preliminary unpublished results of Koval. According to these

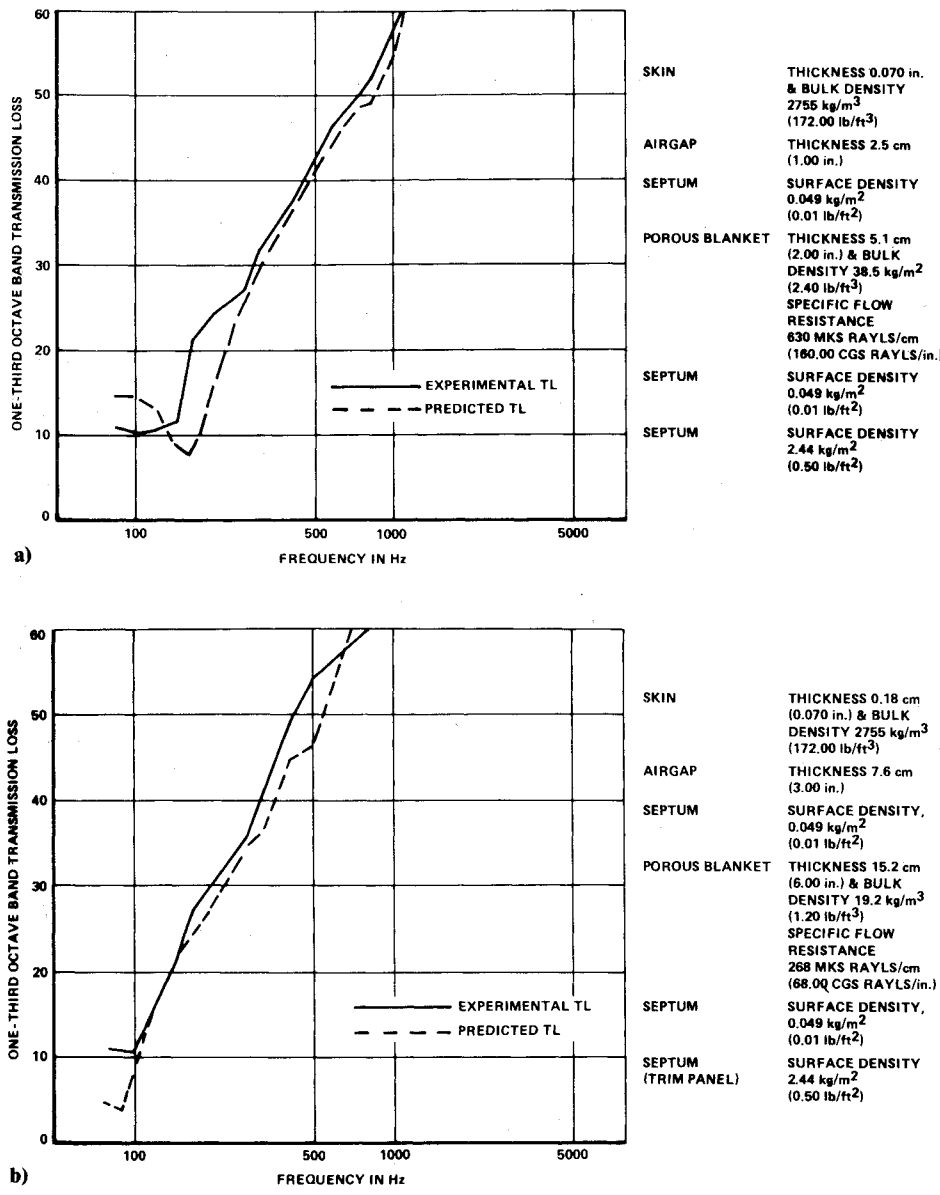

Fig. 6 Multilayer panel transmission loss (reverberant room to reverberant room). a) One panel plus 3-in. double-wall treatment (1-in. airgap plus 2-in., 2.4-lb/ft^3 blanket plus 0.50-psf trim panel). b) Bare panel plus 9-in. double-wall treatment (3-in. airgap plus 6-in., 1.2-lb/ft^3 blanket plus 0.50-psf trim panel).

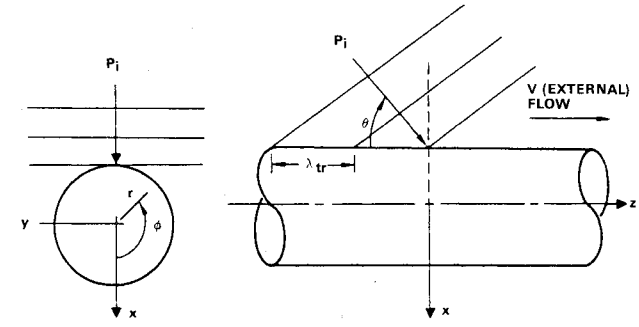

Fig. 7 Geometry of sound waves impinging on a cylindrical shell in high-speed flight.

studies, the presence of the floor causes circumferential coupling of the primitive cosine-type shell vibration modes used in the present theory, as outlined in Appendix A.

Layered Panel Transmission Loss Results

The results of Fig. 6 verify one of the essential premises of double-wall noise reduction, namely, the achievement of 60 dB of increased TL for each decade increase of frequency above the double-wall resonance frequency. Notice by comparison that the TL of the untreated panel (Appendix B) shows a 20-dB increase of TL per decade in accordance with the classical single-wall mass law.

The results in Figs. 6a and 6b show generally good agreement between theory and flat, multilayered-panel test data for reverberant random incidence conditions. As discussed before, this situation is nearly representative of plane-wave transmission at angles near normal incidence. The theory appears to slightly underpredict the test results, as shown in Fig. 6b for the 22.8-cm (9-in.) double wall between 200 and 630 Hz. Note that the data cover a fairly wide range of parameters. The double-wall spacing varies from 7.6 to 22.8 cm (3 to 9 in.), the blanket bulk density varies from 19.2 to 38.4 kg/m^3 (1.2 to 2.4 lb/ft^3), and the specific flow resistance varies from 268 to 630 MKS Rayls/m (68 to 160 Rayls/in.). The cases of Figs. 6a and 6b simulate a 2.4-kg/m^2 (0.5-psf) trim panel at wall spaces of 7.6 cm (3 in.) and 22.8 cm (9 in.), respectively. One can see the shift in the double-wall resonance frequency from calculated values of about 160 Hz for the 7.6-cm (3-in.) double wall, to about 100 Hz for the 22.8-cm (9-in.) double wall. The fiberglass blankets apparently provide more dissipation at the double-wall resonance frequency than the theory indicates, since the test data do not show the sharp minimum TL predicted by the theory at the double-wall resonance frequency. In calculating the double-wall resonance frequency in the presence of a

fiberglass blanket, one needs to determine an "effective" airgap width. This effective airgap width is automatically determined by the various blanket and airgap impedance expressions given in Appendix B. Computer results show that the effective airgap is wider than the apparent width (net wall space minus the blanket thickness) because the blanket is porous.

Applications of Results to Design

Reference 1 shows how an advantageous effect is obtained by application of the heavy, 0.15-m (6-in.) spaced double-wall, noise-control concept for propfan-powered aircraft, which are characterized by high blade passage frequencies, well above the double-wall resonance frequency of about 40 Hz. As a note of caution, however, in most conventional propeller aircraft the blade passage frequencies range from 50 to 100 Hz. For these aircraft, the double-wall spacing between the outer skin and the inner trim panel is typically 5.1 to 8.9 cm (2 to 3.5 in.) and is about one-half filled with a fiberglass blanket for thermal insulation. This situation is characterized by a higher double-wall resonance frequency, in the range of about 150 Hz for fuselages with minimal treatment, and the typical transmission loss spectrum shape is like Fig. 6a. The absolute TL values at low frequency are, however, much higher, typically about 40 dB for a cylindrical shell in its stiffness control regime. Because the lower propeller harmonics may be below the double-wall resonance frequency, the double-wall effect could be unfavorable at conventional propeller blade passage frequencies, tending to decrease TL compared to that of the basic shell structure. The double-wall treatment may, however, improve the A-weighted SPL by suppressing higher harmonic tones.

Computational Cost Aspects

The present method permits the calculation of interior noise levels for the first ten harmonics for a cost of about $4 for each sidewall configuration. Typically, the parametric studies like those in Ref. 1 would investigate a single set of outer wall structural parameters in combination with six trim panel surface density values and in combination with three different assumed distributions for the harmonics of the external sound field. This total of 18 interior noise evaluations would cost typically about $72, or $4 per individual configuration, a very modest cost which permits the routine study of many configuration parameters. Thus the method is highly cost effective for preliminary studies.

Concluding Remarks

The present paper has described an idealized but useful method of analysis of fuselage sidewall noise reduction. The transmission loss of the untreated structure is taken to be the lower envelope of 1) Koval's theory for cylindrical shells or 2) the transmission loss of the flat skin panels which are bounded by the stiffeners. The stiffeners are smeared to define an equivalent monocoque structure for the shell theory analysis. This procedure is considered to be valid at low frequencies where the wavelengths are large compared to the panel dimensions. At high frequencies the panel transmission tends to dominate. One of the present authors has recently published some new results considering the effects of discrete spatial periodicity of the stiffeners,[9] and he has also described the effect of discretely spaced stringers.[10] Some of these results were previewed in Appendix D of Ref. 2. In general, Refs. 9 and 10 confirm the validity of the smeared-stiffener assumption at low frequencies and define additional resonances at high frequency due to coupling between the shell and the stiffeners.

The effect of layered sidewall treatments is analyzed using the flat multilayer-panel theory of Beranek and Work[7] as implemented by Cockburn and Jolly,[6] subject to several corrections described by the present authors in Appendix E of Ref. 2. The present application of the flat-panel sidewall theory takes into account the membrane forces caused by a pressurized cylindrical shell; otherwise, panel curvature is neglected. The application of flat-panel multilayer wall theory is considered to be valid because the wall spacing is small compared to either the shell radius, the acoustical wave lengths, or the panel bay dimensions.

In the final analysis, the validity of the method is supported by laboratory test data shown in this paper. The present theory is obviously a highly simplified model of the real problem; however, the general agreement between theory and test data is considered good enough to be used for preliminary design studies.

One aspect of special note is that the present theory models the structural response as a traveling wave which has the same axial wave number as the acoustical excitation. This assumption says that the structural response is dominated by a classical condition of "coincidence" with the incident oblique plane acoustical wave. In practice, the shell response is a linear combination of many vibration modes with axial mode shapes of the standing wave type, for which the lowest possible axial wave number for a fuselage of length, L, is

$$k_{z\min} = \pi/L \tag{4}$$

Furthermore it is likely that the response of these very long wavelength axial modes will be small because the generalized force input caused by the distributed external noise signature (which is concentrated near the propeller disk plane) will not be nearly as strong as for a coincident mode. Therefore, as a practical matter, excluding all axial wave numbers below $5\pi/L$ may be justified.

Koval's theory[4,5] on the other hand, yields a zero value for the axial wave number at normal incidence [90-deg graze angle; see Eq. (A3) in Appendix A]. For zero axial wave number, all of the stiffness and axial membrane tension terms in the shell equations go to 0; this explains the very low transmission losses predicted at low frequency. Real structures of finite length have a stiffness control regime at low frequencies. These factors are believed to explain the underprediction of low-frequency noise reduction near normal incidence shown in Fig. 4c, and also the reverberant, random incidence results of Fig. 5.

With regard to the prediction of noise reduction, recent unpublished calculations by one of the authors indicate that Eq. (1) is excessively conservative because of gradients of the intensity of the interior sound field which tend to carry the acoustical energy away from the propeller disk plane to be absorbed over the entire cabin length. This yields lower peak noise levels, roughly approximating the results which would have been obtained if the absorption coefficient was assumed to be unity. Numerically, the result is similar to the results of Rennison et al.[11] in this aspect.

Appendix A: Outline of Koval Theory for Cylindrical Shell TL

Koval's theory, described in Refs. 4 and 5, calculates TL for an oblique plane convected with an external steady flow. In application of the theory, the amplitude of the free-field external sound pressure is adjusted to empirical data. The incident sound wave satisfies the convected wave equation. This determines the axial wave number of the external sound pressure. Using Koval's notation (with $\bar{z}$ as the axial coordinate and the incoming sound wave in the x-z plane of Fig. 7), the incident sound pressure at the cylinder surface $r=a$ is

$$p_i = P_i \exp[j(\omega t - k_z z)] \sum_{m=0}^{\infty} \epsilon_m (-j)^m J_m(k_{1r} r) \cos m\phi \tag{A1}$$

where J_m is a Bessel function of the first kind.

The scattered sound wave accounting for the reflection pressure at the cylinder surface is

$$p_s = \exp[j(\omega t - k_z z)] \sum_{m=0}^{\infty} A_m H_m^{(2)}(k_{1r} r)\cos m\phi \qquad \text{(A2)}$$

where $H_m^{(2)} = J_m - jY_m$ is a Hankel function of the second kind and Y_m is a Bessel function of the second kind.

The shell response is calculated as follows: 1) The sum of the incident plus scattered sound pressure is the forcing term for the radial component of the shell displacement. 2) The radial displacement is assumed to be a traveling wave in the axial direction like Eqs. (A1) and (A2). 3) The axial wave number of the displacement is required to be equal to that of the external sound field; therefore, if θ is the grazing angle of incidence (Fig. 7), then

$$k_z = k_{1z} = (\omega/c_1)\cos\theta/(1+M\cos\theta) \qquad \text{(A3)}$$

This is an important assumption in which the shell response is governed by a "coincidence condition" matching the axial wave speeds of the flexural waves in the shell to the axial wave speed in the external sound field.

The transmitted interior sound pressure is in the form of a radially inward traveling wave, using the approach of Smith,[12] and the radial dependence is of the form

$$p_2 = \exp[j(\omega t - k_z z)] \sum_{m=0}^{\infty} B_m H_m^{(1)}(k_{2r} r)\cos m\phi \qquad \text{(A4)}$$

where $H_m^{(1)} = J_m + jY_m$ is a Hankel function of the first kind.

This formulation is logarithmically singular at $r=0$ and is not intended to be a realistic interior description. Instead, it is used as a basis for calculating the energy absorbed by the interior as a fraction of the energy in the free-field incident sound wave. Equation (4) is used to calculate an impedance of the contents of the shell (the air inside the cabin). This impedance is added to the mechanical impedance of the shell using the Gurney-Lurie Flugge Byrne equations.[13] Koval's mechanical impedance result is given by the following equation:

$$Z_m^{SH} = j\omega m_{SH}(\omega_R/\omega)^2 \Delta/[(1-\nu^2)(A_{12}A_{21} - A_{11}A_{22})] \qquad \text{(A5)}$$

where Δ is the determinant of matrix A_{ij}.

A closed form expression for the shell impedance is given in Ref. 4 for monocoque shells. Expressions for the matrix elements, A_{ij}, including the smeared stiffeners, are given in Appendix C based upon Ref. 5. Appendix C includes some minor algebraic corrections to Ref. 5.

Koval combines the shell impedance with the content impedance Z_m^C to obtain the mth circumferential modal impedance Z_m so that

$$Z_m = Z_m^{SH} + Z_m^C \qquad \text{(A6)}$$

where from Eq. (A4) it can be shown that

$$Z_m^C = \frac{j\omega\rho_2 H_m^{(1)}(k_{2r}a)}{k_{2r}[H_m^{(1)}(k_{2r}a)]_{x_{2r}}} \qquad \text{(A7)}$$

where the subscript x_{2r} in Eq. (A7) denotes the partial derivative with respect to $x_{2r} = k_{2r}a$ and where

$$k_{2r} = (\omega/c_2)\{1 - (c_2/c_1)^2[\cos\theta/(1+M\cos\theta)]^2\}^{1/2} \qquad \text{(A8)}$$

and the axial wave number is constant through each medium; therefore

$$k_{2z} = k_z = k_{1z} \qquad \text{(A9)}$$

Finally, the cylinder transmission loss (TL) is defined as

$$\text{TL} = 10\log_{10}\left(\frac{\text{incident power}}{\text{absorbed power}}\right) \qquad \text{(A10a)}$$

$$= 10\log_{10} Q^{(a)} \qquad \text{(A10b)}$$

where the incident power per unit cylinder length is

$$\frac{\partial(\text{incident power})}{\partial z} = \frac{2aP_I^2}{\rho_1 c_1}\sin\theta \qquad \text{(A11a)}$$

The absorbed power per unit length is

$$\frac{\partial(\text{absorbed power})}{\partial z} = a\frac{p_{2m}p_{2m}^*}{Z_m^c} \qquad \text{(A11b)}$$

where p_{2m} is the mth coefficient of Eq. (A4), and the asterisk denotes the complex conjugate. Using Eqs. (A1-A9) Koval deduces the following expressions

$$Q^a = \sum_{m=0}^{\infty} \frac{(2\epsilon_m/x_{1r})r_m^c r_m^s}{(r_m + r_m^s)^2 + (\chi_m + \chi_m^s)^2} \qquad \text{(A12)}$$

$$r_m = \text{Re}(z_m), \qquad \chi_m = \text{Im}(z_m), \qquad x_{1r} = k_{1r}a \qquad \text{(A13)}$$

$$r_m^s = \frac{2/x_{1r}}{(J_m')^2 + (Y_m')^2} \qquad \text{(A14)}$$

$$x_m^s = \frac{-(J_m J_m' + Y_m Y_m')}{(J_m')^2 + (Y_m')^2} \qquad \text{(A15)}$$

$$z_m = (Z_m/\rho_1 c_1)\sin\theta(1 + M_1\cos\theta) \qquad \text{(A16)}$$

$$r_m^c = \text{Re}(Z_m^c/\rho_1 c_1) \qquad \text{(A17)}$$

$$k_1 = \frac{\omega/c_1}{1 + M_1\cos\theta} \qquad \text{(A18)}$$

Koval's theory describes the TL due to the gross radial motion of the cylindrical shell including the stiffeners. Because of the assumption that the stiffeners are smeared into the skin of an equivalent orthotropic monocoque shell, the resultant shell motion approximates the motion of the rings and stringers of the actual stiffened shell. Depending upon the panel bay dimensions, pressurization, and the mass and stiffness of the individual panels, it is possible for the individual panels to cause a lower transmission loss owing to incremental skin panel motion between the stiffeners.

Appendix B: Description of Skin Panel and Added Treatment Layer Transmission Loss

Skin Panel

The free-field TL of an isolated skin panel is given by

$$\text{TL} = 20\log_{10}[P_I/P_T] \qquad \text{(B1)}$$

where the incident to transmitted sound pressure ratio is

$$\frac{P_I}{P_T} = \frac{1}{2}\left[1 + \frac{Z_p\cos\beta_2}{Z_2} + \frac{\rho_1 c_1\cos\beta_2}{\cos\beta_1(1+M\sin\beta_1)Z_2}\right] \qquad \text{(B2)}$$

The reader will recall from Fig. 2 and the related discussion that the method chooses the lower bound for TL, either Eq. (A10) or (B1), as indicated in Fig. 2.

Note that β now denotes the classical angle of incidence with respect to the surface normal, and Z_2 is the termination

impedance of the receiving airspace approximated as

$$Z_2 = \rho_2 c_2 \tag{B3}$$

The panel impedance is

$$Z_p = \left(\frac{\omega_0^2}{\omega}\right) m\eta + \frac{\omega^3 D\eta \sin^4\beta_1}{c_1^4 (1+M\sin\beta_1)^4}$$

$$+ j\left(\omega m - \frac{\omega_0^2 m}{\omega} - \frac{\omega_0^3 D}{c_1^4} \frac{\sin^4\beta_1}{(1+M\sin\beta_1)^4}\right) \tag{B4}$$

where ω_0 is the fundamental frequency of the skin having dimensions a and b in the axial and circumferential direction and m is the panel surface density,

$$\omega_0 = \frac{\pi}{(m)^{1/2}} \left[\left(\frac{P_{ax}}{a^2} + \frac{P_{cir}}{b^2}\right) + D\pi^2 \left(\frac{1}{a^2} + \frac{1}{b^2}\right)^2\right]^{1/2} \tag{B5}$$

Transmission Loss of Added Treatment Layers

The elements of add-on noise-control treatment considered are shown in Fig. 1. They include 1) a viscoelastic damping treatment bonded to the outer skin; 2) an airgap (required for cooling air heat transfer); 3) a fiberglass blanket for thermal insulation; 4) an inner trim panel; and 5) an optimal impervious septum which can be inserted between the blanket and airgap. Items 2 to 4 are part of the standard sidewall construction of an aircraft cabin, but they might be modified for noise-control purposes if it is deemed to be advantageous.

Viscoelastic Damping Treatment

The viscoelastic damping treatments are assumed to be an integral part of the outer wall skin adding mass but do not increase the stiffness of the outer wall. Therefore Eqs. (B1-B5) still describe their performance, except that the terminating impedance is based on fluid properties in the airgap between the outer skin and the fiberglass blanket.

The Airgap and Fiberglass Blankets

The ratio of incident to transmitted pressure is given by

$$\frac{P_1}{P_T} = \frac{\cosh\left[bd\cos\phi + \coth^{-1}(Z_2\cos\phi/Z_B)\right]}{\cosh\left[\coth^{-1}(Z_2\cos\phi/Z_B)\right]} \tag{B6}$$

where d represents d_{Ag} or d_{bl} (see Fig. 1), and b is the complex propagation constant for blankets according to Beranek.[14]

$$b = \left(\frac{j\omega(1/K)(Z_1 Z_2 - \tau_{12}^2 Y)}{Z_2 + (1-Y)\tau_{12}}\right)^{1/2} \tag{B7}$$

where

$$Z_1 = R_1 + j\omega\rho_0 k, \qquad Z_2' = Z_2' + R_2(1-Y)\partial/\partial x \cong Z_2'$$

$$Z_2' = R_1 Y + j\omega[\rho_m + (k-1)\rho_0 Y], \qquad \tau_{12} = R_1 + j\omega(k-1)\rho_0$$

and where ρ_m and ρ_0 are the bulk densities of the blanket and of the air in the blanket, k is the structure factor, and Y is the porosity of the blanket. Z_B is the characteristic impedance of the layer in question. For blankets

$$Z_B = -jKb/\omega Y \tag{B8}$$

For airspaces

$$b = -j\omega/C_A \qquad Z_B = Z_A = \rho_A C_A \tag{B9}$$

The input impedance for a blanket or airgap is

$$Z_{in} = \frac{Z_B}{\cos\phi} \coth\left[bd\cos\phi + \coth^{-1}\left(\frac{Z_2\cos\phi}{Z_B}\right)\right] \tag{B10}$$

where ϕ is the angle of incidence of the wave passing through the blanket.

Equations (B6) and (B10) represent modifications to the method of Cockburn and Jolly.[6]

The Interior Trim Panel

The pressure ratio across the trim panel is calculated by the relation

$$P_1/P_T = 1 + Z_p\cos\beta_2/Z_2 \tag{B11}$$

where $Z_2 = \rho_2 c_2$ is the interior airspace termination impedance. The trim panel impedance Z_p is calculated from Eq. (B4) with appropriate values of mass and stiffness for the trim panel. The fundamental natural frequency of the trim panel is calculated from Eq. (B5), with the membrane force terms P_{ax} and P_{cir} equal to 0, since the trim panel is vented to the cabin. The classical angle of incidence of the sound wave within each layer is calculated by equating the axial wave number, $k_z^{(n)}$, within the nth interior layer, to the exterior axial wave number given by Eq. (A3) in terms of the external graze angle θ; the result is

$$\sin\beta_n = (c_n/c_1)\cos\theta/(1+M\cos\theta) \tag{B12}$$

In the case of the fiberglass blanket, the complex propagation constant b given by Eqs. (B7) defines a complex propagation velocity

$$c_{bl} = \omega/\mathrm{Re}(b) \tag{B13}$$

The value defined in Eq. (B13) would then be used in Eq. (B12) to define the angle of incidence ϕ within the blanket which is required for Eqs. (B6) and (B10). Therefore, within the blanket,

$$\sin\phi = \omega\cos\theta/[c_1 \mathrm{Re}(b)(1+M\cos\theta)] \tag{B14}$$

Septa

In some high-frequency, noise-control applications, a septum is useful and is considered to be a special case of the panel with the following impedance expression

$$Z_{sep} = j\omega m \tag{B15}$$

A heavy lead vinyl sheet with negligible stiffness is an example of a septum.

Multiple-Layered Configurations

The complex ratio of sound pressures across n layers is given by

$$\left[\frac{P_1}{P_T}\right] = \left[\frac{P_1}{P_2}\frac{P_2}{P_3}\frac{P_3}{P_4}\frac{P_n}{P_T}\right] \tag{B16}$$

The transmission loss is then given by Eq. (B1).

In Koval's theory for the bare shells only, P_T in this case represents the interior pressure in the cabin denoted as P_2, as shown in Eq. (A4).

The termination impedances needed for each of the layer expressions are obtained by working outwards from the cabin interior. The configuration shown in Fig. 1 is used as an example. The termination impedance for the trim panel is $Z_2 = \rho_2 c_2$, based on the properties of the air in the cabin. The termination impedance for the fiberglass blanket is the sum of

$\rho_2 c_2$ plus the trim panel impedance. The termination impedance of the airgap is the input impedance of the blanket

$$Z_{2ag} = Z_{bl,in} = (Z_B/\cos\phi)\coth(\arg)$$

$$\arg = bd\cos\phi + \coth^{-1}(Z_{tr}\cos\phi/Z_B) \qquad \text{(B17)}$$

where Z_{tr} equals the sum of the mechanical impedance of the trim panel plus $\rho_2 c_2$.

The airgap input impedance is the termination impedance required for the outer skin in Eq. (B11) in the case of a built-up wall. Thus

$$Z_{2sk} = Z_{ag,in} = (Z_A/\cos\phi)\coth(\arg)$$

$$\arg = bd\cos\phi + \coth^{-1}(Z_{bl,in}\cos\phi/Z_A) \qquad \text{(B18)}$$

Here, Z_A and Z_B are the characteristic impedances of the airgap and the blanket, respectively.

Appendix C: Cylindrical Shell Impedance Relationships

In Ref. 5 Koval gives the equations for the shell impedance in terms of the elements of a 3×3 matrix, A_{ij}, which are derived from the Flugge-type shell equations. A variational method developed by Rosen and Singer[15] was used to smear out the stiffeners. The matrix elements A_{ij} are taken from Ref. 5, including a few algebraic corrections to the elements A_{11}, A_{22}, and A_{23}. The corrected equations are

$$A_{11} = (1+\mu_1+\tfrac{1}{2}P')x_{mz}^2 + \tfrac{1}{2}(1-\nu)(1+k) - P'm^2 - (1-\nu^2)\omega^2/\omega_R^2 \qquad \text{(C1)}$$

$$A_{12} = A_{21} = \tfrac{1}{2}(1+\nu)mx_{mz} \qquad \text{(C2)}$$

$$A_{13} = A_{31} = k\tfrac{1}{2}(1-\nu)m^2x_{mz} + (\chi_1 - k)x_{mz}^3 - (\nu+P')x_{mz} \qquad \text{(C3)}$$

$$A_{23} = A_{32} = (\chi_2 + k\eta_{02})m^3 - (1+\mu_2+\chi_2+k\eta_{02}-P')m - k[\tfrac{1}{2}(3-\nu)+\eta_{t1}]mx_{mz}^2 \qquad \text{(C4)}$$

$$A_{22} = (1+\mu_2-P')m^2 + [\tfrac{1}{2}(1-\nu)(1+3k) + k\eta_{t1} + \tfrac{1}{2}P']x_{mz}^2 - (1-\nu^2)(\omega/\omega_R)^2 \qquad \text{(C5)}$$

$$A_{33} = (1+\mu_2+2\chi_2) + m^2(P'-2\chi_2) + \tfrac{1}{2}P'x_{mz}^2 + k[(1+3\eta_{02}) - 2m^2(1+2\eta_{02}) + (1+\eta_{01})x_{mz}^4 + (2+\eta_{t1}+\eta_{t2})m^2x_{mz}^2 + (1+\eta_{02})m^4] - (1-\nu^2)\omega^2/\omega_R^2 \qquad \text{(C6)}$$

The above equations use Koval's notation of Ref. 5 where

$$x_{mz} = k_{1z}a\,, \quad P' = \Delta p_0 a(1-\nu^2)/Eh\,, \quad k = h^2/12a^2 \qquad \text{(C7)}$$

$$\omega_R = (E/\rho^{SH})^{1/2}/a\,, \quad \mu_j = (1-\nu^2)E_jA_j/Eb_jh \qquad \text{(C8)}$$

$$\chi_j = (1-\nu^2)E_jA_je_j/Eb_jha\,, \quad D = Eh^3/12(1-\nu^2) \qquad \text{(C9)}$$

$$\eta_{0j} = E_jI_{0j}/Db_j\,, \quad \eta_{tj} = G_jJ_j/Db_j \qquad \text{(C10)}$$

where

A_j = cross-sectional area of stiffener
E_j = elastic modulus of the stiffener
G_j = shear modulus of the stiffener
e_j = eccentricity of the stiffener
I_{0j} = moment of inertia of the stiffener (about the middle surface of the shell)
J_j = torsion constant of the stiffener
b_j = spacing between stiffeners

Subscript 1 refers to the stringers and subscript 2 refers to the rings.

The general notation is as follows:

a = shell radius
h = skin thickness
ν = Poisson's ratio
E = elastic modulus of the skin
ρ^{SH} = density of the skin of the shell
k_{1Z} = k_Z is the axial wave number (Appendix A)
ω_R = ring frequency, rad/s
D = plate modulus of the skin material
Δp_0 = cabin pressure differential

References

[1] Revell, J.D., Balena, F.J., and Koval, L.R., "Interior Noise Control by Fuselage Design for High-Speed Propeller-Driven Aircraft," *Journal of Aircraft*, Vol. 19, Jan. 1982, pp. 39-45.

[2] Revell, J.D., Balena, F.J., and Koval, L.R., "Analytical Study of Interior Noise Control by Fuselage Design Techniques on High-Speed, Propeller-Driven Aircraft," NASA CR-159222, April 1980.

[3] Revell, J.D. and Tullis, R.H., "Fuel Conservation Merits of Advanced Turboprop Transport Aircraft," NASA CR-152096, Aug. 1977.

[4] Koval, L.R., "On Sound Transmission Into a Thin Cylindrical Shell Under Flight Conditions," *Journal of Sound and Vibration*, Vol. 48, No. 2, 1976, pp. 265-275.

[5] Koval, L.R., "On Sound Transmission Into a Thin Cylindrical Shell Under Flight Conditions," AIAA Paper 76-549, July 1976.

[6] Cockburn, J.A. and Jolly, A.C., "Structural-Acoustic Response, Noise Transmission Loss and Interior Noise Levels of an Aircraft Fuselage Excited by Random Pressure Fields," USAF, AFFDL-TR-68-2, Wright-Patterson Air Force Base, Ohio, Aug. 1978.

[7] Beranek, L.L. and Work, G.A., "Sound Transmission Through Multiple Structures Containing Flexible Blankets," *Journal of the Acoustical Society of America*, Vol. 21, No. 4, July 1949, pp. 419-428.

[8] Cremer, L., "Insulation of Airborne Sound by Rigid Partitions and Insulation of Impact Sound," WADC-TR-52-04, Vol. I, Supplement I, Wright-Patterson Air Force Base, Ohio, 1955.

[9] Koval, L.R., On Sound Transmission Into a Stiffened Cylindrical Shell With Rings and Stringers Treated as Discrete Elements," *Journal of Sound and Vibration*, Vol. 71, No. 4, Aug. 1980, pp. 511-521.

[10] Koval, L.R., Effect of Longitudinal Stringers on Sound Transmission Into a Thin Cylindrical Shell," *Journal of Aircraft*, Vol. 15, No. 12, Dec. 1978, pp. 816-821.

[11] Rennison, D.C., Wilby, J.F., and Wilby, E.G., "Prediction of the Interior Noise Levels of High-Speed Propeller-Driven Aircraft," AIAA Paper 80-0998, June 1980.

[12] Smith, P.W. Jr., "Sound Transmission Through Thin Cylindrical Shells," *Journal of the Acoustical Society of America*, Vol. 29, No. 6, June 1957, pp. 721-729.

[13] Kraus, H., *Thin Elastic Shells*, John Wiley and Sons, New York, 1967, p. 222.

[14] Beranek, L.L., "Acoustical Properties of Homogeneous, Isotropic Rigid Tiles and Flexible Blankets," *Journal of the Acoustical Society of America*, Vol. 19, No. 4, July 1947, pp. 556-568.

[15] Rosen, A. and Singer, J., "Vibrations of Axially-Loaded Stiffened Cylindrical Shells," *Journal of Sound and Vibration*, Vol. 34, No. 3, 1974, pp. 357-378.